# Comprehensive study on the degradation progress of crumb tire rubber during the preparation of terminal blended rubberized asphalt binder

Meng, Yuanyuan; Ye, Xiangqian; He, Fuqiong; Chen, Zhipeng; Hu, Chichun; Lin, Peng

**DOI**
10.1016/j.jclepro.2023.137916

**Publication date**
2023

**Document Version**
Final published version

**Published in**
Journal of Cleaner Production

**Citation (APA)**
Meng, Y., Ye, X., He, F., Chen, Z., Hu, C., & Lin, P. (2023). Comprehensive study on the degradation progress of crumb tire rubber during the preparation of terminal blended rubberized asphalt binder. *Journal of Cleaner Production*, *417*, Article 137916. https://doi.org/10.1016/j.jclepro.2023.137916

Journal of Cleaner Production 417 (2023) 137916

Contents lists available at ScienceDirect

Journal of Cleaner Production

journal homepage: www.elsevier.com/locate/jclepro

# Comprehensive study on the degradation progress of crumb tire rubber during the preparation of terminal blended rubberized asphalt binder

Yuanyuan Meng [a], Xiangqian Ye [a], Fuqiong He [b], Zhipeng Chen [a], Chichun Hu [a,*], Peng Lin [c]

[a] College of Civil Engineering & Transportation, South China University of Technology, Guangzhou, Guangdong, 510640, China
[b] Guangdong Dr. Road Traffic Technology Co., Ltd, Guangzhou, Guangdong, 510630, China
[c] Section of Pavement Engineering, Department of Engineering Structures, Faculty of Civil Engineering and Geosciences, Delft University of Technology, Netherlands

ARTICLE INFO

Handling Editor: Jian Zuo

*Keywords:*
Crumb tire rubber
Terminal blend rubberized asphalt binder
Resource recycling
Degradation
Desulfurized
Depolymerized

ABSTRACT

Terminal blended rubberized asphalt binder (TB) technology, which blends crumb tire rubber (CR) with asphalt under high interaction conditions, offers a promising waste tire recycling solution for pavement construction. By precisely controlling the degradation progress of CR, it is possible to prepare TB with specific property requirements. However, the degradation progress of CR and its impact on TB property during the TB preparation process remain ambiguous. This hinders the potential for efficient preparation of TB with specific property requirements. This study aims to understand the degradation progress of TB by analyzing binders, soluble fractions, and insoluble fractions obtained at various interaction durations. Microscopic analysis characterizes the chemical composition, morphology, and molecular weight distribution of insoluble and soluble fractions, while macroscopic analysis evaluates the solubility, viscosity, compatibility, and mechanical properties of binders. The results reveal that the degradation of CR during the preparation of TB consists of a desulfurization reaction, depolymerization reaction, and release behavior (carbon black and fillers). Depending on the degradation progress of CR, the interaction process can be classified into three stages: initial (desulfurization reaction dominant stage), middle (depolymerization reaction dominant stage), and last (release behavior dominant stage). The desulfurization reaction of CR is almost completed in the initial stage. The depolymerization reactions and release behavior occur throughout the process. The most pronounced depolymerization reactions occur in the initial stage for natural rubber and in the middle stage for synthetic rubber, while the most significant release behavior occurs in the last stage. Accordingly, in the initial stage, TB shows a rapid evolution in macro properties due to the significant development of degradation reactions, specifically, the notable improvement in viscosity, compatibility, and low-temperature properties, as well as the substantial deterioration in high-temperature properties. In the middle stage, the degradation reaction develops further but slower, with TB exhibits a further but slower evolution in macro properties. In the last stage, the degradation reaction is almost completed, and TB shows a gradual stabilization of macro properties. The findings are expected to achieve precise control of CR degradation progression, which offers the possibility of efficient preparation of TB with specific properties, thus advancing the application of CR in pavement engineering.

## 1. Introduction

According to statistics, more than 17 million tons of waste tires are discarded worldwide every year (Gagol et al., 2015). Improper disposal of large quantities of waste tires results in environmental pollution, fire threats, infectious diseases, etc. (Ramarad et al., 2015). In addition, discarding waste tires is a great waste of resources. Hence, from the perspective of resource recycling and environmental protection, seeking potential ways to recycle waste tires is an important and urgent issue. Grinding waste tires into crumb tire rubber (CR) for application as an asphalt modifier in pavement construction has proven to be a promising solution for resource recycling.

The conventional crumb tire rubber modified asphalt binder (RB) is produced by blending CR with asphalt binder (AB) at approximately 180 °C (Ghavibazoo et al., 2016). Throughout the blending process, the polymer network of CR particles absorbs the light components (linear aliphatic chains) from the AB phase. As a consequence, the volume of CR particles expands while the content of light components in the AB phase decreases (Ghavibazoo et al., 2013c; Yao et al., 2015). This interaction

* Corresponding author.
*E-mail address:* cthu@scut.edu.cn (C. Hu).

https://doi.org/10.1016/j.jclepro.2023.137916
Received 9 April 2023; Received in revised form 5 June 2023; Accepted 25 June 2023
Available online 26 June 2023

**Nomenclature**

| | |
|---|---|
| TB | Terminal blend rubberized asphalt binder |
| RB | Conventional crumb tire rubber modified asphalt binder |
| AB | Asphalt binder |
| CR | Crumb tire rubber |
| NR | Natural rubber |
| SR | Synthetic rubber |
| CB | Carbon black |
| TGA | Thermogravimetric analysis |
| SEM | Scanning electron microscope |
| FTIR | Fourier transform infrared spectroscopy |
| GPC | Gel permeation chromatography |
| RV | Rotational viscometer |
| FM | Fluorescence microscopy |
| RTFOT | Rolling thin film oven test |

process is characterized by swelling behavior. The resulting RB demonstrates exceptional resistance to rutting, cracking, and fatigue, as well as notable capabilities in noise reduction and cost saving, etc. (Presti, 2013). However, the swelling behavior exhibited by CR directly leads to an augmented viscosity of RB, thereby giving rise to challenges in terms of handling, pumping, and compaction processes (Wu et al., 2016). Furthermore, the elevated viscosity necessitates higher construction temperature, consequently triggering the emission of harmful substances during the preparation and construction process, such as benzothiazole, cyclohexyl mercaptan, and methyl-thiophene (Yang et al., 2019). Consequently, this not only leads to excessive energy consumption but also results in environmental pollution. Additionally, the substantial proportion of insoluble rubber particles, characterized by distinct chemical properties (molecular weight and polarity) and physical characteristics (density and solubility) compared to AB, contributes to the poor compatibility of the binder (Ma et al., 2021). Such inadequate compatibility of RB exacerbates the phase segregation between the CR phase and AB phase, both during storage or transportation (Wang et al., 2017). These deficiencies significantly impede the application of CR in pavement engineering. Therefore, the exploration of methods for producing low-viscosity, homogeneous, and high-performance rubberized asphalt binder represents a crucial avenue for advancing this technology.

As widely recognized, CR is a composite polymer material formed through the polymerization of the rubber hydrocarbon backbone from natural rubber (NR) and synthetic rubber (SR). This polymerization process involves cross-linking of the rubber hydrocarbon backbone using sulfurs, reinforcement with fillers, as well as the incorporation of processing oil to enhance its workability and softness (Dong and Zhao, 2018; Song et al., 2018). Researchers found that, during the preparation process with high interaction conditions (typically 220~260 °C, ≥4000 rpm), with the AB phase serving as a solvent, the CR phase can be sufficiently degraded and dissolved in the AB phase. Degradation, as a counteractive process to polymerization, breaks the cross-linked network structure of CR through desulfurization reactions (cleavage of the sulfur bonds between the rubber hydrocarbon backbone) and depolymerization reactions (breakage of C–C and C═C bonds in rubber hydrocarbon backbone), in addition, accompanies the release behavior of the filler (Billiter et al., 1997; Dong and Zhao, 2018; Wang et al., 2020b). As a result, the differences between the CR phase and the AB phase gradually diminish, which holds the potential to expand the applicability and enhance the utilization of CR in pavement engineering.

Terminal blend rubberized asphalt binder (TB) technology, which involves blending CR with AB under high interaction conditions, is regarded as a promising approach to improve the aforementioned challenges associated with RB (Tang et al., 2019; Wang et al., 2021). In the process of TB preparation, the swelling behavior of CR is superseded by the degradation behavior (Abdelrahman and Carpenter, 1999). Accordingly, the degraded rubber hydrocarbons dissolve into the AB phase, resulting in an improved viscosity and compatibility of the binder. However, the degradation of the CR elastomer leads to a loss of elastic properties and a sacrifice in the binder's high-temperature performance (Huang et al., 2017). Effectively managing the degradation degree of cross-linked CR during the interaction processing is a critical factor in obtaining a binder that exhibits desirable solubility, compatibility, and mechanical performance.

Current researches on TB preparation primarily focus on investigating the various interaction conditions that influence the degradation behavior of CR, as well as the resulting properties of TB, as shown in Table 1. Such as the influence of raw materials and processing parameters on the degradation of CR, the degradation rate of CR, the degradation products of CR, the methods for accelerating CR degradation, and the evolution of TB properties. According to the conclusions present in Table 1, variations in these interaction conditions can lead to different degradation progress (rates and degrees) of CR, resulting in TB with different properties. Therefore, in the preparation process of TB under different interaction conditions, precise control of the CR's degradation progress is the crucial approach for producing high-quality products that

**Table 1**
Overview of studies on the TB preparation.

| Conditions | Conclusions | References |
|---|---|---|
| Type of asphalt | Asphalt containing a higher content of light molecular weight components facilitates the degradation of CR. | Billiter et al. (1997); Irena et al. (2006) |
| Source of CR | NR and SR both show degradation behavior but exhibit different rates and magnitudes. NR is more prone to dissolving into the asphalt compared to SR. | Abdelrahman and Carpenter (1999); Liu et al. (2019); Yao et al. (2015) |
| Size of CR | Blends obtained with different CR sizes exhibit similar properties under high interaction conditions. | Billiter et al. (1997) |
| Processing temperature, duration, and mixing rate | Enhanced temperature, extended processing duration, and intensified shear rates can promote the degradation of CR. An interaction temperature of 220 °C led to degradation as the governing process. | Billiter et al. (1997); Ghavibazoo et al. (2013c); Ragab et al. (2013) |
| Evolution of viscosity, compatibility, and rheological properties | Degradation of the CR results in a contribution in viscosity, compatibility, low and intermediate temperature performance, but the reduction in high-temperature performance of the binder. | Abdelrahman and Carpenter (1999); Huang et al. (2017); Tang et al. (2016); Wen et al. (2020) |
| Degradation rates of CR | The degradation rate of CR exhibits a significant initial increase and subsequently stabilizes gradually. | Abdelrahman and Carpenter (1999); Billiter et al. (1997) |
| Degradation products of CR | The polymers released by CR in asphalt undergo gradual degradation, resulting in the breakdown of larger molecules into smaller ones. | Ghavibazoo et al. (2016); Li et al. (2017); Ragab et al. (2018) |
| Pre-treatment of CR | The degradation rate of CR can be accelerated by pre-treatment measures, such as solvents, radiation, mechanochemical extrusion, etc. | Dong and Zhao (2018); Li et al. (2022); Xu et al. (2022) |

meet specific climate and traffic requirements. However, there is still ambiguity surrounding this approach, including the degradation progression of each CR component, the morphological alterations in CR, and the impact of CR degradation on binder components and properties throughout TB preparation.

The objective of this study is to investigate the degradation progress of CR (microscopic) at different interaction stages during the TB preparation process, as well as the resulting evolution of TB properties (macroscopic). A comprehensive investigation of this objective is expected to enable precise control of CR degradation progression under various interaction conditions, thereby providing a reference for the preparation of TB with specific properties. The investigation holds practical significance in advancing the application of TB. To achieve a comprehensive understanding of this objective, the binders, soluble fractions, and insoluble fractions (separated by Soxhlet extraction) obtained from different interaction stages were analyzed respectively. Specifically, on the microscopic, the chemical component and microscopic morphology of the insoluble fractions were characterized via thermogravimetric analysis (TGA) and scanning electron microscope (SEM). The chemical component and molecular weight distribution of the soluble fractions were investigated by Fourier transform infrared spectroscopy (FTIR) and gel permeation chromatography (GPC). On the macroscopic, the solubility, viscosity, compatibility, and mechanical properties of the binders were evaluated by Soxhlet extraction, rotational viscometer (RV) test, storage stability test, fluorescence microscopy (FM) test, and rheological performance test, respectively. Meanwhile, the connection between the micro and macro properties of TB during the preparation process was discussed.

## 2. Materials and methodology

### 2.1. Materials

The AB with a penetration of 60/70, supplied by Shell Asphalt Co., Ltd. (China), was used to prepare all the specimens in this study. The basic properties of the AB are presented in Table 2. The CR with a particle size of 40 mesh (0.425 mm) was manufactured from grinding waste truck tires at ambient temperature. The physical properties of the CR are listed in Table 3. Tetrahydrofuran, purchased from Aladdin Biochemical Technology Co., Ltd. (Shanghai, China) with a purity of 99.9%, was used in the solubility and GPC tests.

### 2.2. Specimen preparation

Prior to preparing the test specimens, the CR was dried to a constant weight by storing it in an oven at 60 °C for 30 min. The AB was preheated to a fluid state at 165 °C. Subsequently, the pre-dried CR was mixed with AB at 20 wt%. Two types of rubberized asphalt binders, denoted RB and TB, were prepared under different interaction conditions. RB was prepared under low interaction conditions, specifically at a temperature of 180 °C and a shearing rate of 5000 r/min for 60 min (Li et al., 2021). To ensure the complete degradation of CR in AB (Billiter et al., 1997; Han et al., 2016), TB was processed under high interaction conditions, including a temperature of 260 °C, a shearing rate of 5000 r/min, and a duration of 360 min. During the preparation process of TB, specimens were obtained at various interaction durations of 5, 15, 30, 60, 120, 240, and 360 min to study the degradation progress of CR in AB at different interaction stages. These specimens were labeled as TB5, TB15, TB30, TB60, TB120, TB240, and TB360, respectively. Notably, the RB and AB were used as the control group. The processing conditions of the specimens are listed in Table 4.

**Table 2**
Basic properties of AB.

| Physical properties | Measured value | Test methods |
|---|---|---|
| Penetration (25 °C,100g, 5s) 0.1 mm | 63.5 | ASTM-D5 |
| Softening point (R&B) °C | 47.8 | ASTM-D36 |
| Ductility (15 °C,5 cm/min) cm | >150 | ASTM-D113 |
| Viscosity (135 °C) Pa·s | 0.390 | ASTM-D4402 |

**Table 3**
Physical properties of CR.

| Indicators | Density (g/cm$^3$) | Moisture content (%) | Metal content (%) | Fiber content (%) |
|---|---|---|---|---|
| Value | 1.12 | 0.48 | 0.034 | 0.51 |

### 2.3. Experiment

To gain a comprehensive understanding of the degradation progress of CR in AB, a series of tests were conducted as depicted in Fig. 1. Each experimental method is described in the following sections. Three replicate tests were performed on each sample.

#### 2.3.1. Solubility test

Soxhlet extraction (Cao et al., 2021; Dong et al., 2018) was performed to separate soluble and insoluble fractions from the specimens at different interaction stages. To be consistent with the GPC test, tetrahydrofuran was used as the solvent to dissolve the soluble fractions, and a polypropylene filter membrane (0.45 μm) was utilized to filter the insoluble fractions. In particular, the portion passing through the filter membrane was defined as the soluble fraction, while the fraction residing on the membrane was defined as the insoluble fraction. The experiment was carried out in the following steps: (1) each specimen ($m_1$, approximately 10 g) was wrapped tightly with filter membrane ($m_2$) and placed in an extractor; (2) Remove the soluble fractions by the extraction process, the process was performed for 48 h until no color changes of the solvent in the Soxhlet siphon were observed; (3) The filter membrane containing the insoluble fractions ($m_3$) was dried in a 60 °C vacuum oven for 3 h and measured until weight maintains constant.

The soluble fractions content of CR was characterized by solubility (S), which was calculated by Eq. (1).

$$S = (1 - (m_3 - m_2) / (20\% \times m_1)) \times 100\% \quad (1)$$

Where: $m_1$ is the initial weight of the specimen, $m_2$ is the weight of the filter membrane, $m_3$ is the weight of the filter membrane containing the insoluble fractions, and 20% is the proportion of CR in the specimens.

#### 2.3.2. Thermal analysis

TGA analysis was utilized to evaluate the changes in the chemical composition of CR during its degradation in AB. The CR or insoluble fractions, approximately 25 mg, were tested by a thermal analyzer (NETZSCH STA 449F3, Germany). The test procedure was implemented according to the specification ISO-99241 (2016), as depicted in Fig. 2a (Step I to Step V).

The weight loss during the TGA was automatically recorded by the instrument, as presented in Fig. 2b. The mass ratio of each component in

**Table 4**
Processing conditions of the specimens.

| Label | CR content (wt.%) | Temperature (°C) | Duration (min) | Shearing speed (r/min) |
|---|---|---|---|---|
| AB | 0 | – | – | – |
| RB | 20 | 180 | 60 | 5000 |
| TB5 | 20 | 260 | 5 | 5000 |
| TB15 | 20 | 260 | 15 | 5000 |
| TB30 | 20 | 260 | 30 | 5000 |
| TB60 | 20 | 260 | 60 | 5000 |
| TB120 | 20 | 260 | 120 | 5000 |
| TB240 | 20 | 260 | 240 | 5000 |
| TB360 | 20 | 260 | 360 | 5000 |

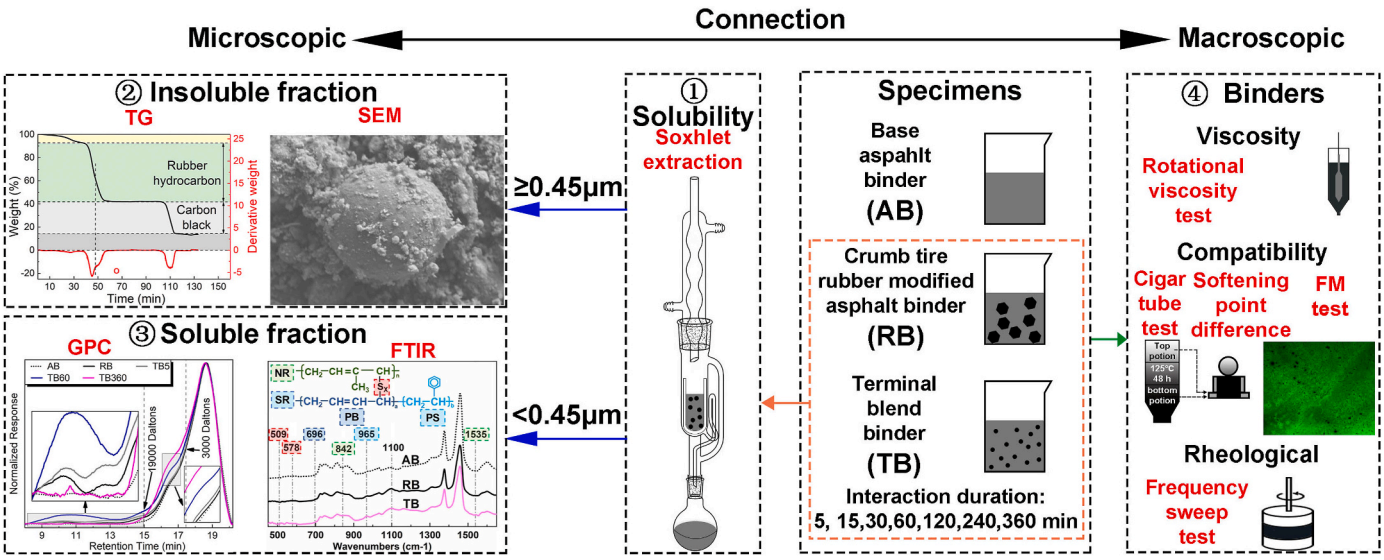


**Fig. 1.** Experimental scheme.

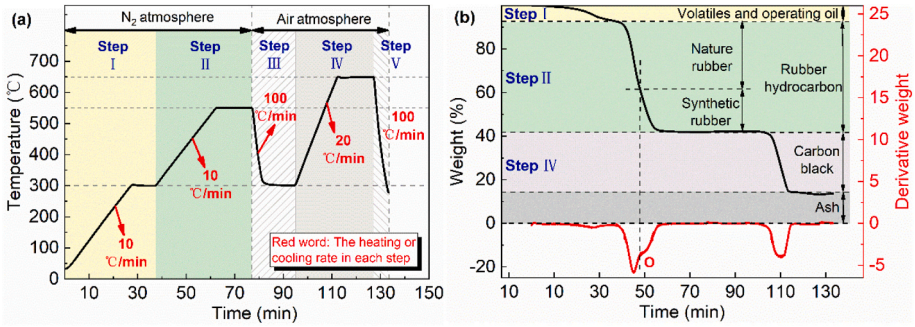


**Fig. 2.** The procedures for the TGA test (a) and the calculation method for determining the component content of CR or insoluble fractions (b).

CR or insoluble fraction was calculated according to the determined decomposition temperature. Specifically, the weight loss in steps I corresponds to the content of volatiles and processing oil. The weight loss in step II is attributed to the decomposition of rubber hydrocarbons. The weight loss in step IV is associated with the combustion of carbon black (CB); and the remaining weight loss is related to ash content (Ma et al., 2021). In addition, the derivative of the thermographs analysis was calculated, correspondingly, the boundary decomposition temperature between NR and SR was determined from the intersection (point O in Fig. 2b) of the two decomposition peaks in the thermographs analysis curve.

The mass ratio of each component in insoluble fraction obtained from the TGA curves were relative values, which should be adjusted by solubility values (calculation according to section 2.3.1) to acquire the absolute content of each component, as shown in Eq. (2):

$$\text{Absolute content (\%)} = \text{Relative content} \times (1\text{- Solubility}) \quad (2)$$

### 2.3.3. Microscopic morphology characterization

The microscopic morphology of CR and insoluble fraction was tested by SEM to characterize the morphological evolution of CR during the degradation process. Before testing, both the CR and insoluble fraction specimens were covered with a fine gold film to ensure a conductive surface and avoid electrostatic artifacts. The instrument (S-3700 N, HITACHI, Japan) was utilized at an accelerating voltage of 20 kV.

### 2.3.4. Molecular weight test

The GPC (1260 Infinity II, Agilent Technology Inc., California, USA) was employed to study the molecular weight distribution of soluble fractions. The specimen was dissolved with tetrahydrofuran for 4 h at a concentration of ~2 mg/ml. The polypropylene filter membrane (0.45 μm) was utilized to separate the soluble fraction from insoluble fractions. The peak area normalization method was used for quantification (Dong and Zhao, 2018).

### 2.3.5. Functional group characterization

The functional groups of soluble fractions were studied by FTIR (NicoletIs5, Thermo Fisher Scientific, USA) in transmission mode. The solution containing the soluble fraction (prepared by GPC test) was dropped on a KBr window, and dried in a 60 °C oven for 30 min to ensure the volatilization of tetrahydrofuran (Ghavibazoo et al., 2015). The scanning range of the infrared spectrum was 400 $cm^{-1}$ to 4000 $cm^{-1}$ with a resolution of 4 $cm^{-1}$ and performed by running 32 scans on each sample. For semi-quantitative analysis of the functional group content, the infrared spectrums were normalized to eliminate the effect of film thickness (Dong et al., 2018).

### 2.3.6. Viscosity measurement

A Brookfield rotational viscometer (DV-II, 27#rotor) was adopted to measure the viscosity of specimens. The RV test was conducted at 135 °C and 165 °C as per the specification of ASTM-D4402 (2015).

### 2.3.7. Compatibility test

The phase separation tendency of the specimen was conducted

according to ASTM-D7173 (2014). A cigar tube containing the specimen was processed according to the steps described in the specification. The softening point of the specimen in the top and bottom portion of the cigar tube was tested respectively, and the softening point difference was calculated. In addition, the microstructure distribution of the specimens at various interaction durations was also investigated by FM (Nikon Y-IDP, Japan). The diluted solution, which was prepared according to the GPC test and without filtering, was utilized to obtain a transmissive specimen in fluorescence mode. Specifically, the diluted solution was dropped onto a glass slide and dried in an oven at 60 °C for 30 min.

#### 2.3.8. Rheological properties test

The rheological properties of specimens over a wide temperature and frequency range were evaluated with a frequency sweep test by a dynamic shear rheometer (Kinexus lab+, Malvern Panalytical, UK). The strain amplitude for the frequency sweep test was within the linear viscoelastic response of the specimen. The frequency range for the frequency sweep test was performed over a range of 0.1 Hz–30 Hz, and the test was conducted at the temperature of 4 °C, 16 °C, 28 °C, 40 °C, 52 °C, 64 °C and 76 °C, respectively. At temperatures of 4 °C, 16 °C, and 28 °C, a plate with a diameter of 25 mm and a gap of 1 mm was employed. For the remaining test temperatures, an 8 mm diameter plate and with a gap of 2 mm was utilized.

#### 2.3.9. Laboratory aging

The aging procedure of AB was simulated by a rolling thin film oven test (RTFOT), which was conducted according to ASTM-D2872 (2004).

## 3. Result and discussion

### 3.1. Solubility of CR

During the interaction, the cross-linked structure of CR is gradually disrupted along with the degradation behavior. Accordingly, the CR phase dissolves into the AB phase, forming the soluble fraction (Wang et al., 2017). The solubility of CR under different interaction conditions is shown in Fig. 3, it can be found that the solubility between RB and TB exhibits significant differences.

Research has indicated that in most cases, the occurrence of swelling behavior is typically accompanied by degradation behavior (Wang et al., 2017). During the interaction process, the light components from the AB phase diffuse into the rubber hydrocarbon network of the CR phase, which results in a swelling behavior and volume expansion of the CR. At a certain point, the swelling of CR reaches equilibrium and the volume of CR ceases to expand, correspondingly, the rubber hydrocarbon network starts to degrade (Irena et al., 2006). The research findings demonstrate that under high interaction conditions, there is a notable increase in the diffusion coefficient, accompanied by a significant decrease in the equilibrium swelling time, therefore, the CR phase can be degraded and dissolved into the AB phase faster and sufficiently (Wang et al., 2019).

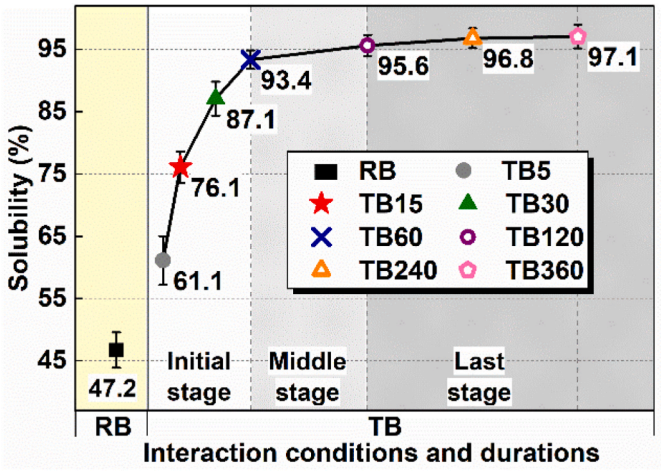


**Fig. 3.** Solubility of CR under different interaction conditions and durations.

As shown in Fig. 3, the solubility of RB is only 47.2%. This is due to the dominant swelling behavior of CR under low interaction conditions, wherein only the outer rubber hydrocarbon that is fully swollen undergoes degradation (Wang et al., 2020a). Additionally, the limited energy available is insufficient to profoundly disrupt the inner network structure of CR, resulting in a comparatively low solubility. In contrast, under high interaction conditions, the swelling behavior is quickly replaced by the degradation behavior, showing a degradation behavior dominated interaction process (Dong et al., 2018; Wang et al., 2017). As depicted in Fig. 3, during the initial stage (0–60 min), the solubility of TB exhibits nearly linear growth, reaching 93.4% at 60 min. This observation indicates that the high thermal energy rapidly breaks the cross-linked structure of CR, leading to the release of numerous fractured rubber hydrocarbons into the AB phase. Subsequently, in the middle stage (60–120 min), the solubility of TB increases gradually, suggesting that the accumulated thermal energy further breaks the network structure of CR, thereby deepening the solubility of CR (Dong and Zhao, 2018; Ghavibazoo et al., 2013a). During the last stage (120–360 min), the solubility of TB remains relatively stable, demonstrating that the rubber hydrocarbon structure has been nearly completely degraded at this stage.

### 3.2. Composition of insoluble components

The relative values regarding the transformation in the chemical composition of cross-linked rubber hydrocarbons before and after degradation are listed in Table 5. The absolute content is calculated based on the relative values, which is considering the effect of solubility, as illustrated in Fig. 4a.

As is known, the cross-linked structure of CR is composed of oil, NR, SR, CB, and ash (including mineral filler and metal impurity, etc.). In particular, cross-linked rubber hydrocarbons (NR and SR) adsorb and tightly wrap the surface of CB, while the ash fills the gaps within the rubber hydrocarbon structure (Dong et al., 2018), as shown in Fig. 4b. During the interaction process, the degraded rubber hydrocarbons chains are peeled off, CB and ash are released from the cross-linked structure, resulting in a reduction in the content of NR, SR, CB, and ash, as observed in Fig. 4a. Accordingly, it can be known that the soluble fraction comprises oil, degraded rubber hydrocarbons, and part of the released CB and ash. The insoluble fraction consists of cross-linked rubber hydrocarbons, CB, and ash (including the wrapped ones and the released ones with particle sizes not less than 0.45 μm).

As seen in Fig. 4a, RB treated under low interaction conditions presents a higher content of insoluble fractions, especially for CB and ash. This is mainly attributed to the low thermal energy, where only the loosed rubber hydrocarbons in the outer layer of CR are degraded. As a result, there are relatively fewer degraded rubber hydrocarbons, as well

**Table 5**
The relative content of chemical components in CR and insoluble fractions.

| Specimen | The relative content of chemical components(%) | | | | |
|---|---|---|---|---|---|
| | Oil | NR | SR | CB | Ash |
| CR | 8.1 | 30.8 | 19.3 | 27.8 | 14.0 |
| RB | 4.8 | 23.2 | 19.0 | 36.4 | 16.6 |
| TB5 | 4.1 | 12.5 | 17.9 | 42.0 | 23.5 |
| TB15 | 3.6 | 10.2 | 16.6 | 45.7 | 23.9 |
| TB30 | 3.5 | 7.5 | 17.1 | 45.4 | 26.5 |
| TB60 | 3.2 | 5.6 | 12.2 | 39.5 | 39.5 |
| TB120 | 3.1 | 3.9 | 8.0 | 35.1 | 49.9 |
| TB240 | 2.5 | 3.1 | 7.3 | 34.1 | 53.0 |
| TB360 | 2.1 | 2.8 | 7.1 | 32.7 | 55.3 |

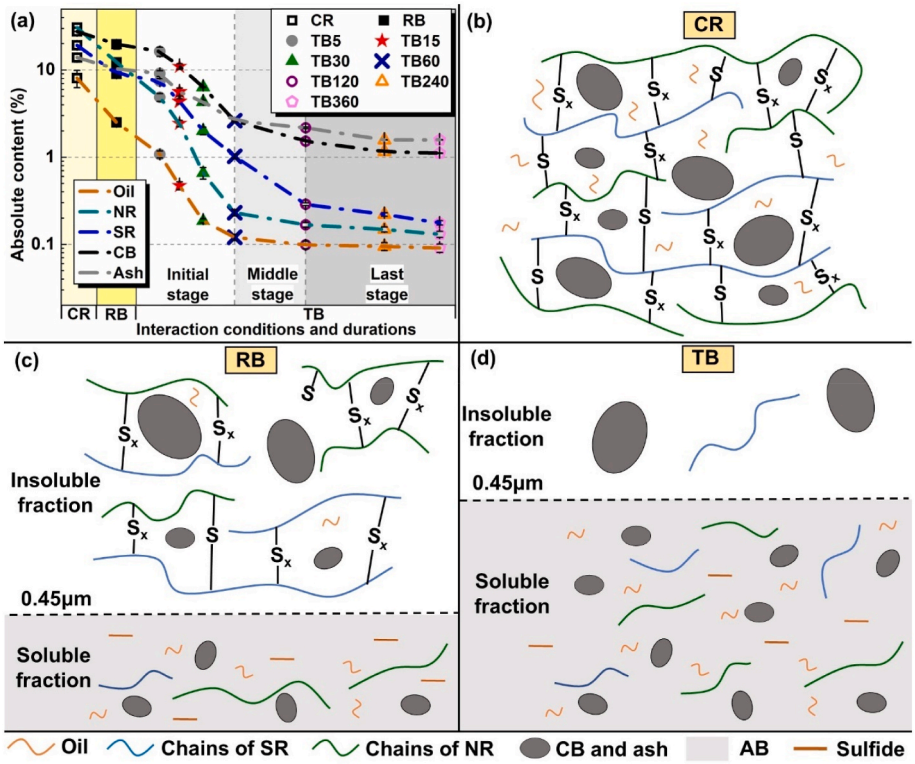


**Fig. 4.** The absolute contents of chemical components for CR and insoluble fractions obtained under different interaction conditions (a), the cross-linked network structure of CR (b), and the schematic diagram of the dissolution processes of RB and TB (c ~ d).

as minor released CB and ash, as illustrated in Fig. 4c.

Compared to the insoluble fractions of RB, the content of the insoluble fractions in TB is dramatically reduced, indicating that the high interaction conditions significantly promote the degradation of CR. Furthermore, each component exhibits a distinct degree of degradation. Firstly, a sharp decrease in oil content is observed during the early interaction stage (within the first 30 min), which is attributed to the good compatibility of the oil with the AB phase. Secondly, the content of NR and SR reaches a relatively stable value by the end of the initial stage (60 min) and middle stage (120 min), respectively. This indicates that the cross-linked structure of rubber hydrocarbon (NR and SR) is almost completely degraded and dissolved into the AB phase at the corresponding stages. These observations can be attributed to the high interaction conditions, which result in a more sufficient and rapid swelling of CR. The accumulated thermal energy further induces more extensive degradation of the swollen cross-linked rubber hydrocarbon, leading to the release of more broken rubber hydrocarbons (Dong et al., 2018), as depicted in Fig. 4d. In addition, the faster degradation rate of NR can be explained by its better compatibility with AB phase (Irena et al., 2006). Thirdly, the content of CB and ash experiences a significant decrease during the initial and middle stages, followed by a relatively stable level in the last stage. This indicates that with the accumulation of energy, more and more rubbery hydrocarbon molecules are fractured, which results in the release of large quantities of wrapped CB and trapped ash into the AB phase.

### 3.3. Microscopic morphology characterization

The surface morphology of the CR and the insoluble fractions obtained from different interaction conditions are listed in Fig. 5. It can be observed that the surface of the original CR particles is smooth, with the presence of sharp edges and corners (Fig. 5a). The surface of the insoluble fractions obtained from RB remains in a relatively smooth state, accompanied by the presence of a few micropores (Fig. 5b), which is attributed to the partial degradation of the rubber hydrocarbon molecules. However, the surface morphology of the TB residue changes considerably as the interaction duration extends from 5 min to 360 min, as shown in Fig. 5c ~ Fig. 5i.

It can be seen that during the pre-initial stage (5 min~15 min, as shown in Fig. 5c and d), the surface of the insoluble fractions undergoes a transformation, becoming rough and developing numerous microporous structures, while the sharp edges and corners disappear. Moreover, with the extension of the interaction duration (15 min~0 min, as shown in Fig. 5e), the surface of the insoluble fractions gradually presents a loose and porous structure. The formation of these microporous structures is attributed to the release of the linear rubber hydrocarbon from the fractured cross-linked rubber hydrocarbon structure (Dong et al., 2018). In addition, the specific surface area of CR increases with the appearance of these microporous. Accordingly, the light components of the AB phase penetrate more easily into the cross-linked rubber hydrocarbon of the CR phase. Consequently, the degradation of CR is accelerated, leading to a progressive loosening in the crosslinked network structure.

With prolonged interaction (60 min~120 min, as shown in Fig. 5f and g), the macro particles of CR degrade into smaller particles, which is a consequence of the continuous breaking, peeling, and dissolution of the rubber hydrocarbon in CR. In addition, small particles show a regular ellipsoidal shape, which may be CB or ash (mineral filler and metal impurity, etc.) wrapped by rubber hydrocarbons.

At the end of the interaction stage (240 min~360 min, as shown in Fig. 5h and i), the roughness of the small particles decreases, and simultaneously, the morphology becomes clearer. According to the figure, the particles show a spherical or ellipsoidal shape, which is the appearance of the CB and mineral fillers in the CR. As is known, the particle size of CB in CR is about tens to hundreds of nanometers (containing few particles larger than 0.45 μm), while the mineral filler is about tens of nanometers to tens of microns (Saowaroj et al., 2002). Therefore, it can be presumed that these residual particles correspond to

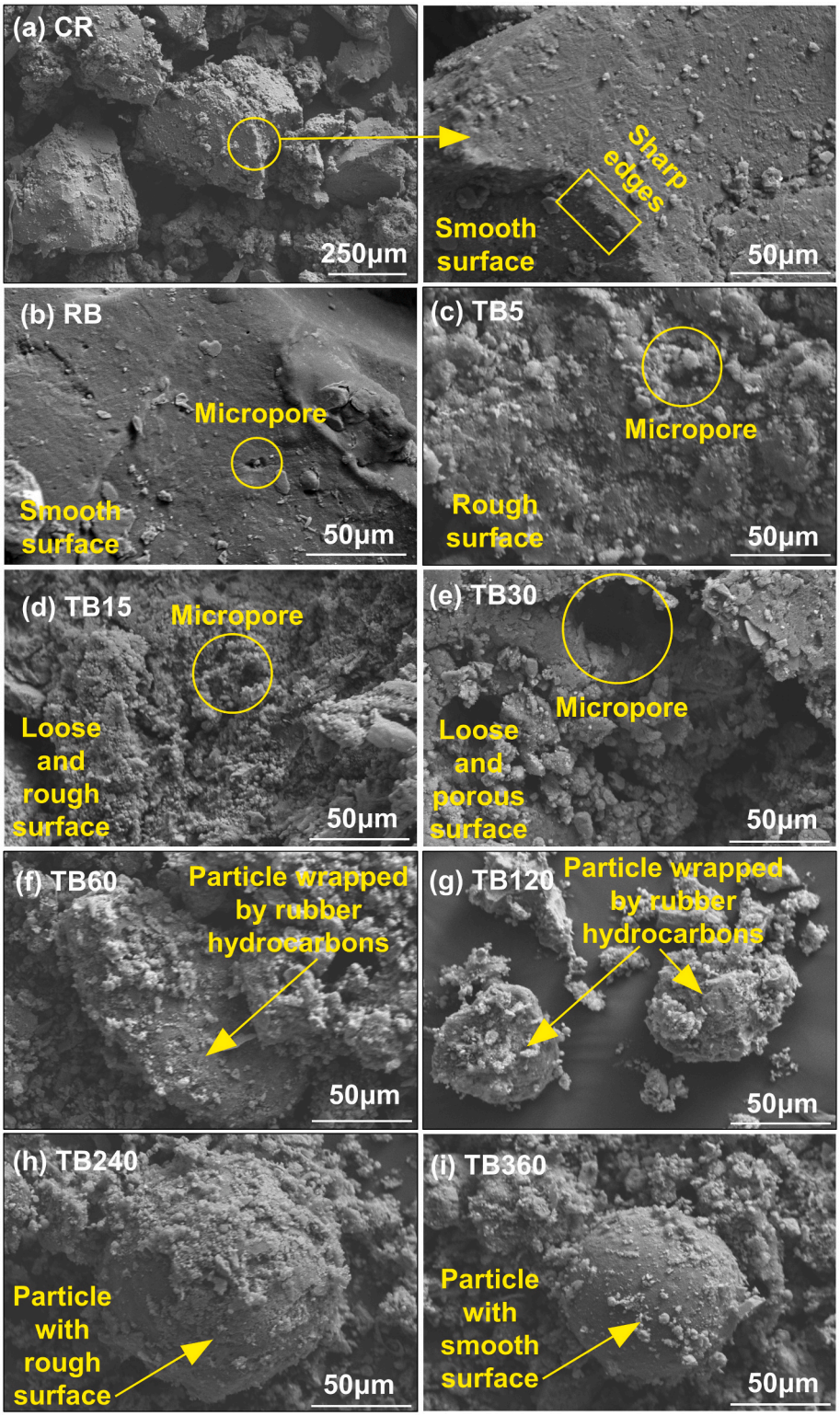


**Fig. 5.** Microscopic morphology of the CR (a) and the insoluble fractions obtained from different interaction conditions (b ~ i).

large-diameter CB and mineral fillers, which cannot pass through the 0.45 μm filter membrane. The gradually exposed CB and mineral filler are due to the continuous degradation and peeling of the rubber hydrocarbon on their surface. At the same time, the degraded hydrocarbons gradually decompose into more linear molecules, eventually dissolving into the AB phase. This phenomenon is consistent with the decreased content of the rubber hydrocarbon, CB, and ash in the TGA results.

### 3.4. Functional group characterization

Infrared spectra of the AB and the soluble fraction obtained from different interaction conditions and durations are shown in Fig. 6a. It can be seen that the positions of the absorption peaks are mostly similar,

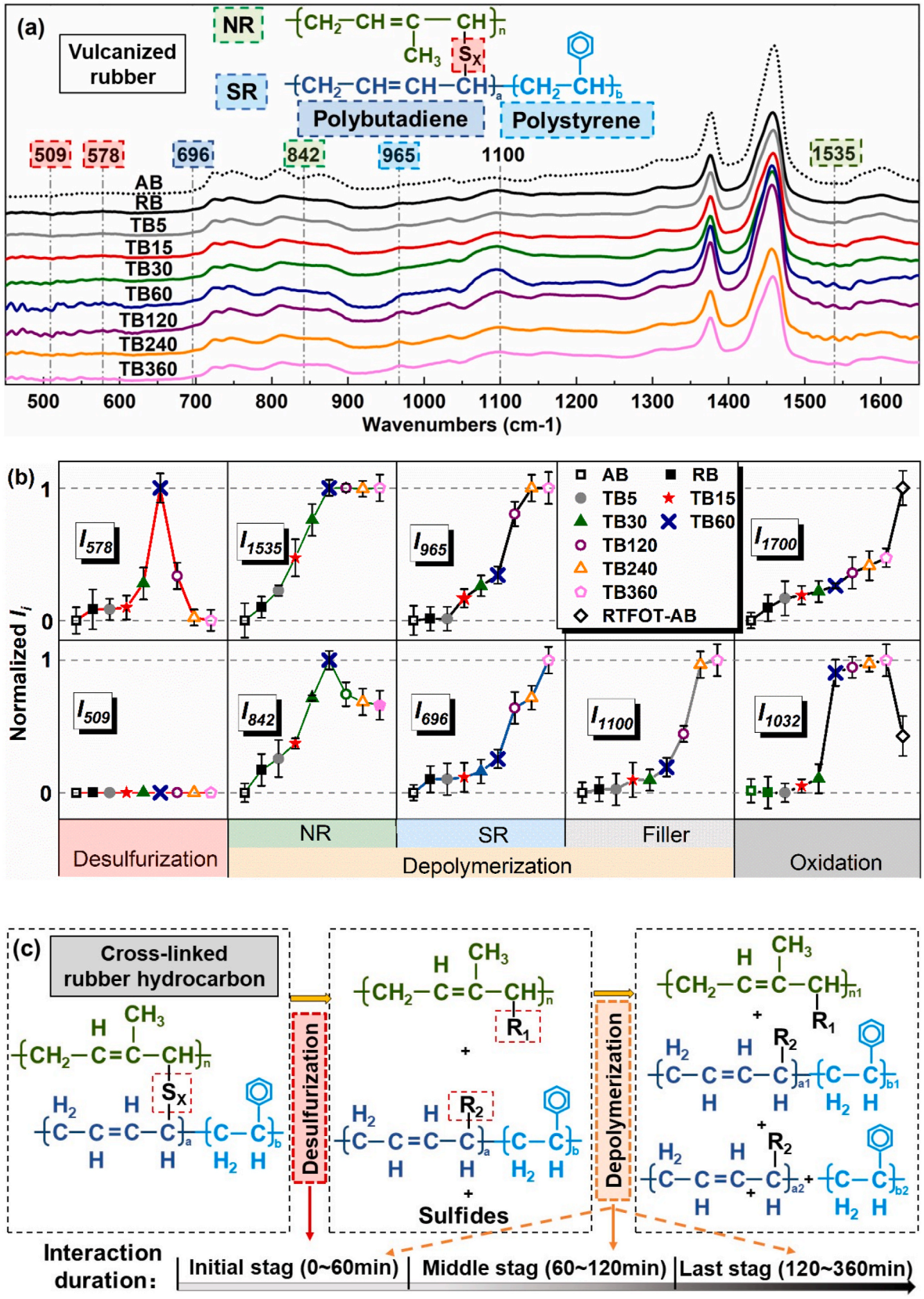


**Fig. 6.** Result of FTIR. (a) Infrared spectra, (b) functional group indexes of each characteristic functional group, (c) degradation mechanism. Note: (1) $S_X$ denotes sulfide, disulfide, and polysulfide bonds; (2) $R_1$ and $R_2$ denote reactive groups; (3) $n > n1$, $a \geq a1$, $a \geq a2$, $b \geq b1$, $b \geq b2$.

accompanied by variations in peak intensities, and the emergence of some new absorption peaks. Therefore, it can be regarded that the condition and duration of interaction influence the degradation products of CR.

The degradation of CR is mainly attributed to the desulfurization reaction (cleavage of sulphury cross-link bonds, e.g. S–S and S–C) and depolymerization reaction (breakage of the backbone of the main chain, e.g. C–C and C═C) (Huang et al., 2017). Since the bond energy of the S–S, S–C, C–C, and C═C bonds in cross-linked rubber hydrocarbon structures are different, as shown in Table 6, it is assumed that these bonds are broken to different degrees at a particular stage (Dong et al., 2018). It can be seen that the S–S and S–C bonds will break first, corresponding to the desulfurization behavior, since they are the most susceptible to thermal and chemical attacks. Afterward, the main chain break into smaller linear molecules, which corresponds to the depolymerization behavior, consequently, the smaller linear molecules are released into the AB phase and further degraded.

To quantitatively analyze the degradation degree of CR under various interaction conditions and durations, the functional group index ($I$) of each characteristic functional group associated with CR is investigated, as shown in Eq. (3):

$$I_i = A_i \Big/ \sum \mathrm{A} \tag{3}$$

where $A$ denotes the integral area with a coordinate axis within a certain molecular range, and $i$ represents the wavenumbers at corresponding characteristic peaks. $\sum A = A_{1700} + A_{1600} + A_{1460} + A_{1376} + A_{1030} + A_{864} + A_{814} + A_{743} + A_{724} + A_{696} + (A_{2953} + A_{2924} + A_{2854})$. In addition, the calculated $I$ was normalized, and the result is shown in Fig. 6b.

As shown in Fig. 6b, regarding the TB specimen, the characteristic peak of the S–S bond at 509 $cm^{-1}$ (Song et al., 2018) is barely visible during the whole interaction process. This can be attributed to the low bond energy of the S–S bond in the cross-linked rubber hydrocarbon molecule, making it easier to break. Furthermore, even after the breakage of the S–S bond, the rubber hydrocarbon still maintains a macromolecular structure and does not dissolve into the AB phase. This is consistent with the previous conclusion that breaking only the cross-linked bonds does not result in a significant soluble fraction (Wu et al., 2017).

It is revealed from Fig. 6b, as the interaction proceeds, the $I$ value corresponding to the C–S bond at 578 $cm^{-1}$ (Song et al., 2018) of the TB specimen initially increases and then decreases, reaching a maximum value at 60 min. In the initial stages (≤60 min), the enhancement in $I_{578}$ implies the breakage of the cross-linked network (as shown by the desulfurization behavior in Fig. 6c). Simultaneously, the long-chain rubber hydrocarbon molecules with sulfide branched chains, as a soluble fraction, gradually dissolve into the AB phase. Afterward, $I_{578}$ starts to decrease and gradually stabilizes, which implies the breakage of sulfide-branched chains. The variation tendency of $I_{578}$ can be attributed to the following reasons. Firstly, in the initial stage, the release of long-chain rubber hydrocarbon molecules with sulfide-branched chains accumulates to the peak, accompanied by partial breakage of sulfide-branched chains. Subsequently, in the middle stage, no more long-chain rubber hydrocarbon molecules with sulfide branched chains are released, while sulfide branched chains are further broken. Then, in the last stage, the breakage of the branched chains is completed.

**Table 6**
The bond energy of different bonds exists in cross-linked rubber hydrocarbon structures.

| Bond types | Bond energy (kJ/mol) |
|---|---|
| S–S | 213 |
| S–C | 259 |
| C–C | 347 |
| C═C | 620 |

As illustrated in Fig. 6a and b, in comparison with the spectra of AB, it is noted that some new absorption peaks appear in the spectra of the TB specimens. Specifically, absorption peaks at 842 $cm^{-1}$, and 1535 $cm^{-1}$ are observed, which correspond to the out-of-plane deformation vibration of C–H in cis double replace C═C and methyl-assisted conjugated double bonds in the vulcanized NR (Ma et al., 2021; Zhao et al., 2021). In addition, characteristic peaks of 965 $cm^{-1}$ and 696 $cm^{-1}$ are also observed, which are related to the trans-alkene in polybutadiene segments and the C–H out-of-plane bending of monoalkylated aromatics in polystyrene segments (Ragab et al., 2018). Notably, the SR molecule is polymerized from polybutadiene and polystyrene segments. The appearance of these peaks means that the long-chain rubber hydrocarbons are gradually depolymerized during the interaction process, as shown by the depolymerization behavior in Fig. 6c. Correspondingly, the NR and SR molecules in the long-chain rubber hydrocarbons are released and dissolved into the AB phase. It can be observed that the intensities of $I_{842}$ and $I_{1535}$ grow fast during the initial stage (0–60 min) and gradually stabilize during the middle stage (60–120 min). This indicates that the release of NR from long-chain rubber hydrocarbons is significant in the initial stage and almost complete in the middle stage. Furthermore, the intensities of $I_{965}$ and $I_{696}$ continue to increase as the interaction duration prolongs, with a faster growth rate observed after 60 min, implying that the number of soluble SR molecules released from the long-chain rubber hydrocarbons is significant during the middle stage, which occurs later than that of NR.

An absorption peak at 1100 $cm^{-1}$ emerges in the spectrum of the TB specimens in comparison with the AB specimen (Fig. 6b), which represents the asymmetric stretching vibration of Si–O–Si. The detected Si–O–Si component is derived from the nano-silica additive in CR (Ma et al., 2021). It is noted that the intensity of $I_{1100}$ exhibits slow growth in the first 60 min, followed by rapid growth after 60 min, and finally stabilizes after 240 min. This result indicates that during the interaction process, the degraded rubber hydrocarbons are continuously peeled off, leading to the release of trapped fillers. Specifically, in the initial stage, insufficient degradation of the rubber hydrocarbons results in a small amount of filler being released. However, in the middle and last stages, as the rubber hydrocarbons undergo further degradation and peeling, a significant amount of trapped inorganic filler is released.

To investigate the aging status of the TB during the interaction process, the intensity of $I$ related to the C═O groups and S═O groups at 1700 $cm^{-1}$ and 1032 $cm^{-1}$ are calculated (Wang et al., 2016), as shown in Fig. 6b. It can be seen, in comparison with AB and RTFOT-AB specimens, the intensities of $I_{1700}$ in the TB specimens present smaller values, which means that no significant aging of the binder occurred during the interaction process. This can be ascribed to the degraded rubber hydrocarbons acting as retarders within the AB, which hinder the penetration of oxygen molecules into the AB and thereby reduce the oxidation rate of the AB (Ghavibazoo et al., 2015). However, the intensities of $I_{1032}$ in the TB specimens increase with the prolongation of interaction duration, especially after 30 min. The asynchronous changes of $I_{1700}$ and $I_{1032}$ suggest that other reactions are taking place apart from binder aging. This phenomenon may be attributed to the oxidation of broken sulfur bonds during the desulfurization process of the cross-linked rubber hydrocarbons, which leads to a significant increase in $I_{1032}$.

It can be seen from Fig. 6a and b, the characteristic peaks of the RB specimen are the same as those of the TB specimens, with only the intensity of the peaks being different. According to the analysis of the spectra of the TB specimens mentioned above, it can be concluded that the desulfurization reactions and depolymerization reactions also take place in the RB specimen. However, the degradation behavior of RB is insignificant due to the low interaction conditions, resulting in weak intensities of the characteristic peaks.

### 3.5. Molecular weight test

From the micro level, the desulfurization and depolymerization reactions of the cross-linked rubber hydrocarbon molecules imply a gradual breakage of the molecular chains (Wu et al., 2017). When rubber chains break into sufficiently small molecules, they can be converted into the soluble fraction, resulting in changes in the molecular weight of the soluble fraction. The chromatograms for the soluble fractions of degraded CR obtained under different interaction conditions are plotted in Fig. 7. The chromatogram is divided into three parts based on the molecular weight ($M_w$). These three parts represent polymers ($M_w \geq 19{,}000$ Da), apparent asphaltenes (3000 Daltons$\leq M_w <$ 19,000 Da), and maltenes ($M_w <$ 3000 Da), respectively (Tang et al., 2019).

The polymer peak can be observed in the soluble fraction of RB, as shown in Fig. 7, indicating that the rubber hydrocarbon molecules are partially degraded under low interaction conditions, which is consistent with the former results of this study. In addition, the apparent asphaltenes peak of the RB specimen is higher than that of the AB specimen. This can be attributed to the rubber particles absorbing the light components from the AB phase during the interaction process, thus, leading to an increase in the average molecular weight of AB phase.

Comparing the chromatograms of TB specimens with those of AB and RB, notable changes in the polymer peaks and apparent asphaltenes peaks can be observed, as depicted in Fig. 7. The chromatograms of the TB specimens reveal polymer peaks at an elution time of 8–14 min, which implies that the cross-linked rubber hydrocarbons are degraded to smaller rubber hydrocarbons and gradually dissolved into the AB phase during the interaction process. In particular, in the initial stage (0–60 min), the polymer peaks show a progressively stronger response, which signifies a rapid degradation of the cross-linked rubber hydrocarbons. Subsequently, in the middle and last stages (60–360 min), the polymer peaks show a weakening trend and eventually disappear, which implies further depolymerization of the soluble polymer into small molecules. In the chromatograms of TB specimens at an elution time of 16–17 min, a progressive strengthening response of the apparent asphalt peak can be observed with the prolongation of the interaction duration. This phenomenon is attributed to the development of the depolymerization reaction of CR, leading to the release of more fractured rubber hydrocarbon molecules (act as apparent asphaltenes) into the AB phase. These findings are consistent with the aforementioned results from TGA and FTIR analyses.

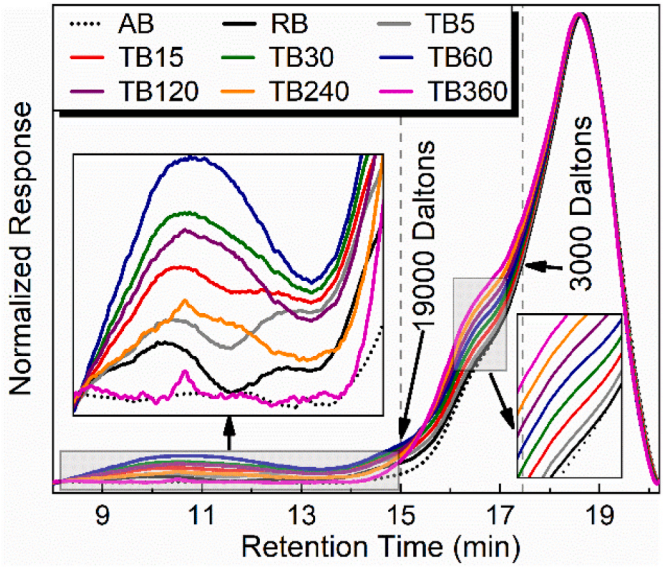


**Fig. 7.** Chromatograms of AB and soluble fractions obtained under different interaction conditions.

### 3.6. Viscosity measurement

During the interaction process of CR with AB, the variations in viscosity are verified as a macroscopic reflection of the swelling and degradation development of CR. The viscosity of the AB and the binders obtained in different interaction conditions is presented in Fig. 8.

The swelling behavior of CR is closely related to the viscosity growth of the binder. This can be attributed to the polymer network of CR absorbing the light components from the AB phase during the interaction process, which subsequently raises the viscosity of the AB phase. Additionally, the volume of CR particles expands, leading to an enhancement in interparticle friction within CR (Peralta et al., 2012), thereby demonstrating a growth in the viscosity of binder. As presented in Fig. 8, the viscosity of RB exhibits a significant increment in comparison to that of the AB, which can be attributed to the dominance of the swelling behavior of CR under low interaction conditions. Similar conclusions were also obtained in previous studies (Li et al., 2018; Presti, 2013).

When the swelling of CR particles reaches equilibrium and accompanies the accumulation of energy, the degradation behavior of CR particles emerges. The degradation process of CR signifies the breakage of the cross-linked molecular structure, resulting in a reduction in particle volume and a consequent decrease in interparticle friction. At the same time, during the degradation process, the light component absorbed by CR is released, which leads to a decrease in the viscosity of the AB phase (Han et al., 2016). Therefore, the degradation process is associated with a decrease in viscosity, contrasting with the increase in viscosity observed during the swelling process.

As depicted in Fig. 8, the viscosity of TB specimens tends to decrease during the interaction process. It can be attributed to the dominant degradation behavior of CR under high interaction conditions, as evidenced by the aforementioned TGA, FTIR, and GPC results (section 3.2~3.4). Moreover, under high interaction conditions, the AB phase exhibits very low viscosity, facilitating easier penetration of the cross-linked network of CR. As a result, the rubber hydrocarbon rapidly reaches swelling equilibrium, which further accelerates the dominance of the degradation reaction (Dong et al., 2012). Specifically, in the initial stage, the cross-linked network structure of the rubber hydrocarbon undergoes significant breakage (the desulfurization reaction is nearly completed), resulting in the gradual peeling off from the CB and filler surface. This leads to a significant reduction in the particle size and a rapid decrease in viscosity. During the middle stage, the long-chain rubber hydrocarbon molecules gradually depolymerize into smaller

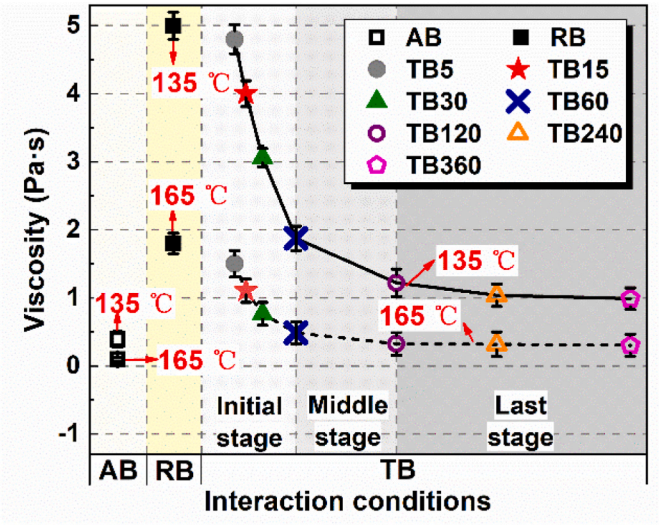


**Fig. 8.** Viscosity of the AB and the binders processed by different interaction conditions.

molecules, further weakening the intermolecular forces. This is manifested by a continuous decrease in viscosity. In the last stage, the depolymerization of rubber hydrocarbon molecules is almost completed, thus exhibiting a stable viscosity.

### 3.7. Compatibility analysis

The compatibility results of RB and TB obtained from the cigar tube test are shown in Fig. 9a. To gain further insight into the mechanism responsible for the improved storage stability under high interaction conditions, FM was utilized to observe the microstructure of all binders, as shown in Fig. 9b~i. In the figure, the green part is the residual tetrahydrofuran (tetrahydrofuran exhibits fluorescence) and the polymer phase (composed of dissolved rubber hydrocarbons polymers) (Xu et al., 2022), while the black ones are CR particles, peeled rubber hydrocarbons, and released fillers.

It is well known that, different densities are exhibited in AB (~1.03 g/cm$^3$), CR particles (1.15 ± 0.05 g/cm$^3$), and fillers released from CR particles (1.8–2.1 g/cm$^3$) (Ghavibazoo et al., 2013b; Wen et al., 2020). These varying densities are responsible for the poor compatibility observed in multi-phase systems.

From Fig. 9a, it is evident that the RB specimen displays the highest difference value, which indicates that phase separation is apparent after processing under low interaction conditions. Furthermore, as shown in Fig. 9b, the CR particles are observed in the form of blocks, indicating that CR and AB still maintain a relatively independent two-phase system. That is to say, the CR phase undergoes only partial degradation, which aligns with the findings from the previous results of this study. Thus, the poor storage stability of the RB specimen can be attributed to the high content of CR, as well as the significant density difference between the CR and AB phases.

In comparison to the RB specimen, the difference value of the TB specimens exhibits a significant decrease with the prolongation of interaction duration, as shown in Fig. 9a. This indicates that high interaction conditions result in a significant improvement in the system's compatibility. It can be found that the difference value remains below 2.5 °C for interaction duration longer than 30 min, which meets the storage stability requirement for modified asphalt. Furthermore, as the interaction duration prolongs, the particles of the TB specimen become noticeably smaller, and the dispersion widens, as depicted in Fig. 9c~i.

In particular, in the initial stage of the interaction process, there is a significant decrease in the difference values (Fig. 9a). As the interaction proceeds, the CR particles gradually transition from a block form to a spot form, accompanied by the emergence of filamentous structures (Fig. 9b~f). These observations align with the findings from the previous sections, indicating the degradation of the cross-linked rubber hydrocarbons. This degradation leads to a reduction in particle size and the appearance of filamentous structures (peeled but undegraded rubber hydrocarbons). As a result, the density difference between the CR phase (with gradually decreasing particle size) and the AB phase (containing degraded rubber hydrocarbons) diminishes, showing an improvement in compatibility.

As the interaction progresses, a gradual disappearance of the filamentous structure can be observed towards the end of the middle stage (Fig. 9g). This can be attributed to the nearly complete depolymerization and dissolution of the rubber hydrocarbon in the AB phase. Subsequently, during the last stage (Fig. 9h~i), only filler particles in a spot form are present. Thus, the compatibility of the system during these stages is highly related to the released filler. Notably, despite the significant density difference between the filler phase and the AB phase, satisfactory compatibility is observed in the middle and late stages (Fig. 9a). This can be attributed to several factors, including the relatively low content of released filler (which accounts for only 5 wt% ~ 10 wt% of the binder according to the TGA results), the small particle size (resulting in a large specific surface area and surface energy), and excellent dispersion in the AB phase.

### 3.8. Rheological properties test

The rheological master curve (reference temperature: 40 °C) of the specimens is constructed over a wide range of frequencies, as depicted in Fig. 10. The complex shear modulus (G*) master curve is established by Williams-Landel-Ferry and Sigmoidal Model, as shown in the following Eq. (4) ~ **(6)**:

$$log\ \alpha_T = -C_1(T - T_0)/(C_2 + (T - T_0)) \tag{4}$$

$$log\ f_R = logf + log\ \alpha_T = logf - C_1(T - T_0)/(C_2 + (T - T_0)) \tag{5}$$

$$log(G^*) = \delta + \alpha \Big/ \left(1 + e^{\beta + \gamma\ log\ f_R}\right) \tag{6}$$

where $\alpha_T$ is shift factor; $T$ is measured temperature (°C); $C_1$ and $C_2$ are constants; $T_0$ is reference temperature (°C); $f_R$ is replaced frequency

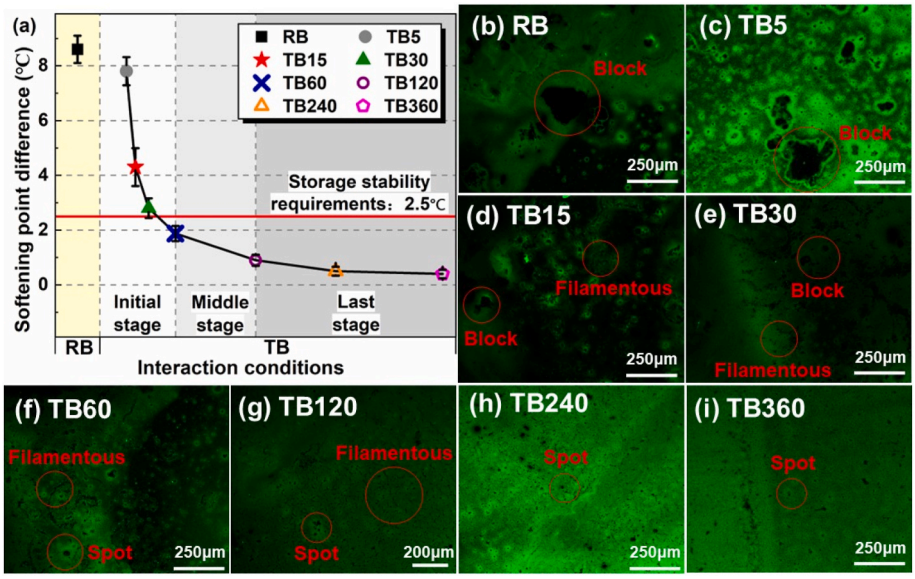


**Fig. 9.** The softening point difference (a) and the microstructure distribution (b ~ i) about the binders processed by various interaction conditions.

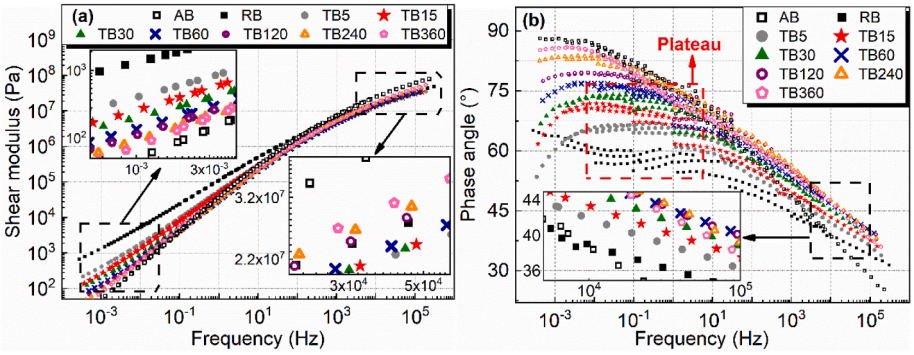


**Fig. 10.** Complex shear modulus master curves (a) and phase angle master curves (b) of the AB and the binders obtained by various interaction conditions.

(Hz); $f$ is measured frequency (Hz); $G^*$ is complex shear modulus (Pa); $\delta$, $\alpha, \beta,$ and $\gamma$ are coefficients (Meng et al., 2022). CR is a complex material from the rheological point of view, to realistically reflect the evolution of the elastic behavior, the phase angle master curve only shifts with $a_T$ (obtained from eq. (4)) in this study, without undergoing the fitting process.

Compared to the AB specimen, the RB specimen exhibits excellent mechanical properties in both the low-frequency region (high temperature) and the high-frequency region (low temperature), as shown in Fig. 10. The enhancement of the mechanical properties at the macroscopic level can be attributed to the swelling behavior of CR phase. This swelling behavior results in the hardening of the AB phase, while the swollen CR phase also functions as an elastic filler in the AB phase. Similar conclusions were obtained in a previous study (Wang et al., 2020b).

During the interaction process under high interaction conditions, the rheological properties of TB specimens exhibit significant differences compared to RB specimens. In particular, as the interaction duration prolongs, the $G^*$ of TB specimens gradually decreases, while the phase angle gradually increases in the low-frequency region. These changes signify the degradation of the binder's high-temperature properties, as shown in Fig. 10. Under high interaction conditions, the swelling behavior of CR is replaced by the degradation behavior, which is indicated in the former analysis. Degradation behavior, from a mechanical perspective, signifies a reduction in the elasticity of the CR particles. Consequently, the function of the CR phase in the AB phase gradually shifts from an elastic filler to an inelastic additive (Ghavibazoo et al., 2014). Moreover, the degradation of the CR particles releases the initially absorbed light components (Wang et al., 2020a), which also contributes to the softening of the binder.

For modified asphalts containing polymers, the phase angle master curve is considered an effective indicator for analyzing the state of the polymer in the binder (Tang et al., 2019). Regarding the RB specimens, a plateau can be observed between $10^{-2}$ Hz and 1 Hz in Fig. 10b. This plateau indicates the presence of elastic polymer networks (Zhou et al., 2021) and indicates a stable balance between the viscous and elastic components of the binder. However, for the TB specimens, it is noted that the plateau region gradually diminishes as the interaction duration extends and disappears during the middle stage. This occurrence is attributed to the progressive degradation of the polymer during the initial and middle stages. In the last stage, the phase angle master curve of TB becomes similar to that of AB, which is due to the complete degradation of the polymer structure. These findings are consistent with the previous results concerning the degradation process of TB specimens.

In the high-frequency region (low temperature), as the interaction progresses, the $G^*$ of TB specimens shows a significant decreasing trend in the initial stage, followed by a slightly increasing trend in the middle and last stages. Conversely, the phase angle shows an opposite trend. This implies that the low-temperature performance of TB improves in the initial stage, but diminishes in the middle and last stages. Taking into account the aforementioned results regarding the degradation process of TB specimens, it can be seen that the desulfurization reaction of rubber hydrocarbons dominates in the initial stage. Thus, the improvement in low-temperature performance may be attributed to the release of long-chain rubber hydrocarbons into the AB phase, thereby enhancing the binder's elasticity (Ragab et al., 2013). The deterioration of low-temperature properties in the middle and last stages can be attributed to the following points. Firstly, the elastic properties of the binder weaken as the long-chain rubber hydrocarbons undergo depolymerization into short-chain rubber hydrocarbons. Secondly, the released CB and fillers contribute to the hardening of the binder. Finally, the volatilization of lighter components within the AB phase, along with slight aging, also contributes to the binder's hardening.

## 4. Summary

In this study, a comprehensive understanding of the evolution in micro properties (degradation progression of CR) and macro properties of TB at different interaction stages during TB preparation is carried out. Table 7 provides a summary of the micro and macro properties evolution of TB during the interaction process. The results indicate a strong connection between the micro and macro properties. Based on the evolution of micro and macro properties, the interaction process can be divided into three stages:

Initial stage: desulfurization reaction dominant stage. The desulfurization reaction is almost completed, accompanied by the depolymerization reaction and insignificant release behavior. Notably, the depolymerization reaction of NR is significant, while the depolymerization reaction of SR is relatively weak. Attributed to the nearly complete desulfurization reaction, the cross-linked network structure of CR is almost entirely degraded into long-chain rubber hydrocarbons, except for the inner layer cross-linked network structure. A substantial amount

**Table 7**
Summary of the TB's property evolution at different interaction stages.

| Property | Interaction stage | | |
|---|---|---|---|
| | Initial stage | Middle stage | Last stage |
| Desulfurization reaction | ★★★★★ | ★ | / |
| Depolymerization reaction (NR) | ★★★★★ | ★ | / |
| Depolymerization reaction (SR) | ★★★ | ★★★★★ | ★ |
| Release behavior (CB and filler) | ★★ | ★★★ | ★★★★★ |
| Solubility | +++ | ++++ | +++++ |
| Viscosity | +++ | ++++ | +++++ |
| Compatibility | +++ | ++++ | +++++ |
| High-temperature performance | – | – | – |
| Low-temperature performance | +++++ | ++++ | +++ |

Note: "★" indicates the progression degree of the response/behavior; "+" indicates the extent of property improvement; conversely, "-" indicates the extent of property deterioration; "/" indicates that this property almost disappears.

of these long-chain rubber hydrocarbons, acting as the polymer phase, dissolve in the AB phase. Thus, at this stage, the significant desulfurization reaction leads to a rapid evolution in the macro properties of TB. Characterized by a substantial reduction in viscosity, a considerable improvement in compatibility, a notable degradation in high-temperature performance, and a significant improvement in low-temperature performance.

Middle stage: depolymerization reaction dominant stage. The depolymerization reaction of NR is almost complete, while the depolymerization reaction of SR is significant, accompanied by the development of release behavior. The polymer phase, composed of long-chain rubber hydrocarbons, undergoes significant depolymerization, resulting in the formation of short-chain rubber hydrocarbons. Correspondingly, the content of the polymer phase in the TB decreases, while the content of apparent asphaltene increases. As a result of the further but slower development of degradation reaction, the viscosity, and compatibility of TB are further improved, while the high-temperature performance undergoes additional deterioration. Notably, the progressive degradation of the polymer results in the loss of elasticity in TB, thereby manifesting as a slight deterioration in low-temperature performance.

Last stage: release behavior dominant stage. The depolymerization reaction of SR is almost completed, accompanied by significant release behavior, with the fastest release rate observed at 120 min. The polymer phase in the TB gradually diminishes, while the content of apparent asphaltene further increases. In addition, a substantial number of CBs and fillers are released. At this stage, the degradation reaction progresses slowly, eventually reaching completion, resulting in the stabilization of macro properties, including stable viscosity and compatibility, as well as slightly reduced high-temperature and low-temperature performance.

## 5. Conclusion

Understanding the degradation progress of CR during the preparation process of TB and its impact on TB properties is of practical significance in guiding the preparation of TB with specific properties. Moreover, this provides possibilities for facilitating the resource recovery of waste tires in pavement engineering. Therefore, the present study provides a comprehensive investigation of the degradation progress (microscopic) of CR and the working properties (macroscopic) of TB during the preparation process, as well as the connection between micro and macro properties. The following conclusions can be arrived at:

(1) Interaction stages can be divided into three stages according to the degradation progress of the cross-linked network of CR during the preparation process of TB: the initial stage (desulfurization reaction dominant stage), middle stage (depolymerization reaction dominant stage), and last stage (release behavior dominant stage). Notably, the desulfurization reaction is almost completed in the initial stage, while the depolymerization reaction and release behavior continue throughout the entire process.
(2) Various components in CR exhibit distinct degradation progresses in different interaction stages. The depolymerization reaction of NR is nearly completed in the initial stage. The depolymerization reaction of SR occurs throughout the interaction process, with the most significant occurrence in the middle stage and completion in the last stage. As the interaction process advances, trapped CBs and fillers are gradually released, demonstrating the most significant release behavior at the last stage.
(3) A sustained evolution of macro properties is observed due to the continuous degradation of CR during the interaction process. Characterized by improvement in viscosity, compatibility, and low-temperature performance, along with degradation in high-temperature performance. In particular, the improvement in low-temperature performance is significant in the initial stage, but exhibits a certain degree of attenuation in the middle and last stages.
(4) Distinct rates of evolution in the macro properties of TB are observed due to the varying degradation progress exhibited by CR in each interaction stage. The significant desulfurization reaction in the initial stage contributes to a rapid evolution in the macro properties of TB. In the middle stage, where degradation reactions progress at a slower rate, the macro properties of TB exhibit a corresponding gradual evolution. During the last stage, the degradation reactions proceed slowly and eventually reach completion, resulting in the stable development of the macro properties of TB.

The research findings can provide insights into the degradation progression of CR during TB preparation under different interaction conditions. This offers possibilities for the efficient design of TB preparation parameters.

## CRediT authorship contribution statement

**Yuanyuan Meng:** Conceptualization, Methodology, Investigation, Experimental program, Writing – original draft, Writing (original draft). **Xiangqian Ye:** Experimental program. **Fuqiong He:** Funding acquisition. **Zhipeng Chen:** Experimental program. **Chichun Hu:** Supervision, Funding acquisition. **Peng Lin:** Conceptualization, Writing – review & editing, Review & editing.

## Declaration of competing interest

The authors declare that they have no known competing financial interests or personal relationships that could have appeared to influence the work reported in this paper.

## Data availability

Data will be made available on request.

## Acknowledgments

This research was supported by the Canton-Hong Kong Joint Research Program (2019A0503004), the Opening Project Fund of Materials Service Safety Assessment Facilities (MSAF-2021-006), and the Shaanxi Provincial Department of Transportation Scientific Research Project (20-14K).

## References

Abdelrahman, M., Carpenter, S., 1999. Mechanism of interaction of asphalt cement with crumb rubber modifier. Transport. Res. Rec. 1661 (1), 106–113. https://doi.org/10.3141/1661-15.
ASTM-D2872, 2004. Standard Test Method for Effect of Heat and Air on Moving Film of Asphalt (Rolling Thin-Film Oven Test).
ASTM-D4402, 2015. Standard Test Method for Viscosity Determination of Asphalt at Elevated Temperatures Using a Rotational Viscometer (PA, West Conshohocken).
ASTM-D7173, 2014. Standard Practice for Determining the Separation Tendency of Polymer from Polymer Modified Asphalt (PA, West Conshohocken).
Billiter, T., Davison, R., Glover, C., Bullin, J., 1997. Production of asphalt rubber binders by high cure conditions. Transport. Res. Rec. 1586 (1), 50–56. https://doi.org/10.3141/1586-07.
Cao, L., Yang, C., Li, A., Wang, P., Zhang, Y., Dong, Z., 2021. Flue gas composition of waste rubber modified asphalt (WRMA) and effect of deodorants on hazardous constituents and WRMA. J. Hazard Mater. 403, 123814 https://doi.org/10.1016/j.jhazmat.2020.123814.
Dong, D., Huang, X., Li, X., Zhang, L., 2012. Swelling process of rubber in asphalt and its effect on the structure and properties of rubber and asphalt. Construct. Build. Mater. 29, 316–322. https://doi.org/10.1016/j.conbuildmat.2011.10.021.
Dong, R., Zhao, M., 2018. Research on the pyrolysis process of crumb tire rubber in waste cooking oil. Renew. Energy 125, 557–567. https://doi.org/10.1016/j.renene.2018.02.133.
Dong, R., Zhao, M., Xia, W., Yi, X., Dai, P., Tang, N., 2018. Chemical and microscopic investigation of co-pyrolysis of crumb tire rubber with waste cooking oil at mild

temperature. Waste Manag. 79, 516–525. https://doi.org/10.1016/j.wasman.2018.08.024.
Gagol, M., Boczkaj, G., Haponiuk, J., Formela, K., 2015. Investigation of volatile low molecular weight compounds formed during continuous reclaiming of ground tire rubber. Polym. Degrad. Stabil. 119, 113–120. https://doi.org/10.1016/j.polymdegradstab.2015.05.007.
Ghavibazoo, A., Abdelrahman, M., Ragab, M., 2013a. Composition analysis of crumb rubber during interaction with asphalt and effect on properties of binder. Int. J. Pavement Eng. 14 (5), 517–530. https://doi.org/10.1080/10298436.2012.721548.
Ghavibazoo, A., Abdelrahman, M., Ragab, M., 2013b. Effect of crumb rubber modifier dissolution on storage stability of crumb rubber modified asphalt. Transport. Res. Rec. 2370 (1), 109–115. https://doi.org/10.3141/2370-14.
Ghavibazoo, A., Abdelrahman, M., Ragab, M., 2013c. Mechanism of crumb rubber modifier dissolution into asphalt matrix and its effect on final physical properties of crumb rubber modified binder. Transport. Res. Rec. 2370 (1), 92–101. https://doi.org/10.3141/2370-12.
Ghavibazoo, A., Abdelrahman, M., Ragab, M., 2014. Effect of crumb rubber dissolution on low temperature performance and aging of asphalt rubber binder. Transport. Res. Rec. 2445 (1), 47–55. https://doi.org/10.3141/2445-06.
Ghavibazoo, A., Abdelrahman, M., Ragab, M., 2015. Evaluation of oxidization of crumb rubber modified asphalt during short term aging. Transport. Res. Rec. 2505 (1), 84–91. https://doi.org/10.3141/2505-11.
Ghavibazoo, A., Abdelrahman, M., Ragab, M., 2016. Changes in composition and molecular structure of asphalt in mixing with crumb rubber modifier. Road Mater. Pavement 17 (4), 906–919. https://doi.org/10.1080/14680629.2016.1138878.
Han, L., Zheng, M., Wang, C., 2016. Current status and development of terminal blend tyre rubber modified asphalt. Construct. Build. Mater. 128, 399–409. https://doi.org/10.1016/j.conbuildmat.2016.10.080.
Huang, W., Lin, P., Tang, N., Hu, J., Xiao, F., 2017. Effect of crumb rubber degradation on components distribution and rheological properties of Terminal Blend rubberized asphalt binder. Construct. Build. Mater. 151, 897–906. https://doi.org/10.1016/j.conbuildmat.2017.03.229.
Irena, G., Robert, S., Franciszek, C., 2006. Molecular Interactions between rubber and asphalt. Ind. Eng. Chem. Res. 45, 3044–3049. https://doi.org/10.1021/ie050905r.
ISO-99241, 2016. Rubber and Rubber Products — Determination of the Composition of Vulcanizates and Uncured Compounds by Thermogravimetry — Part 1: Butadiene, Ethylene-Propylene Copolymer and Terpolymer, Isobutene-Isoprene, Isoprene and Styrene-Butadiene Rubbers (Switzerland).
Li, B., Huang, W., Tang, N., Hu, J., Lin, P., 2017. Evolution of components distribution and its effect on low temperature properties of terminal blend rubberized asphalt binder. Construct. Build. Mater. 136, 598–608. https://doi.org/10.1016/j.conbuildmat.2017.01.118.
Li, D., Leng, Z., Zou, F., Yu, H., 2021. Effects of rubber absorption on the aging resistance of hot and warm asphalt rubber binders prepared with waste tire rubber. J. Clean. Prod. 303, 127082 https://doi.org/10.1016/j.jclepro.2021.127082.
Li, J., Xiao, X., Chen, Z., Xiao, F., Amirkhanian, S.N., 2022. Internal de-crosslinking of scrap tire crumb rubber to improve compatibility of rubberized asphalt. Sustain. Mater. Techno. 32, e00417 https://doi.org/10.1016/j.susmat.2022.e00417.
Li, P., Jiang, X., Ding, Z., Zhao, J., Shen, M., 2018. Analysis of viscosity and composition properties for crumb rubber modified asphalt. Construct. Build. Mater. 169, 638–647. https://doi.org/10.1016/j.conbuildmat.2018.02.174.
Liu, G., Liang, Y., Chen, H., Wang, H., Komacka, J., Gu, X., 2019. Influence of the chemical composition and the morphology of crumb rubbers on the rheological and self-healing properties of bitumen. Construct. Build. Mater. 210, 555–563. https://doi.org/10.1016/j.conbuildmat.2019.03.205.
Ma, J., Hu, M., Sun, D., Lu, T., Sun, G., Ling, S., Xu, L., 2021. Understanding the role of waste cooking oil residue during the preparation of rubber asphalt. Resour. Conserv. Recycl. 167, 105235 https://doi.org/10.1016/j.resconrec.2020.105235.
Meng, Y., Hu, C., Tang, Y., Großegger, D., Qin, W., 2022. Investigation on the erosion mechanism of simulated salt conditions on bitumen. Construct. Build. Mater. 334, 127267 https://doi.org/10.1016/j.conbuildmat.2022.127267.
Peralta, J., Silva, H., Hilliou, L., Machado, A., Pais, J., Christopher, W., 2012. Mutual changes in bitumen and rubber related to the production of asphalt rubber binders. Construct. Build. Mater. 36, 557–565. https://doi.org/10.1016/j.conbuildmat.2012.06.030.
Presti, D., 2013. Recycled tyre rubber modified bitumens for road asphalt mixtures: a literature review. Construct. Build. Mater. 49, 863–881. https://doi.org/10.1016/j.conbuildmat.2013.09.007.
Ragab, M., Abdelrahman, M., Ghavibazoo, A., 2013. Performance enhancement of crumb rubber modified asphalts through control of the developed internal network structure. Transport. Res. Rec. 2371 (1), 96–104. https://doi.org/10.3141/2371-11.
Ragab, M., Abdelrahman, M., Ghavibazoo, A., 2018. Enhancing the crumb rubber modified asphalt's storage stability through the control of its internal network structure. Int. J. Pavement Res. Technol. 11 (1), 13–27. https://doi.org/10.1016/j.ijprt.2017.08.003.
Ramarad, S., Khalid, M., Ratnam, C.T., Chuah, A.L., Rashmi, W., 2015. Waste tire rubber in polymer blends: a review on the evolution, properties and future. Prog. Mater. Sci. 72, 100–140. https://doi.org/10.1016/j.pmatsci.2015.02.004.
Saowaroj, C., Aopeau, i., Nuchanat, N., Pranut, P., 2002. Effects of particle size and amount of carbon black and calcium carbonate on curing characteristics and dynamic mechanical properties of natural rubber. J. Met. Mater. Miner. 12 (1), 51–57.
Song, P., Wu, X., Wang, S., 2018. Effect of styrene butadiene rubber on the light pyrolysis of the natural rubber. Polym. Degrad. Stabil. 147, 168–176. https://doi.org/10.1016/j.polymdegradstab.2017.12.006.
Tang, N., Huang, W., Xiao, F., 2016. Chemical and rheological investigation of high-cured crumb rubber-modified asphalt. Construct. Build. Mater. 123, 847–854. https://doi.org/10.1016/j.conbuildmat.2016.07.131.
Tang, N., Lv, Q., Huang, W., Lin, P., Yan, C., 2019. Chemical and rheological evaluation of aging characteristics of terminal blend rubberized asphalt binder. Construct. Build. Mater. 205, 87–96. https://doi.org/10.1016/j.conbuildmat.2019.02.008.
Wang, H., Liu, X., Apostolidis, P., Erkens, S., Scarpas, T., 2019. Numerical investigation of rubber swelling in bitumen. Construct. Build. Mater. 214, 506–515. https://doi.org/10.1016/j.conbuildmat.2019.04.144.
Wang, H., Liu, X., Apostolidis, P., Erkens, S., Skarpas, A., 2020a. Experimental investigation of rubber swelling in bitumen. Transport. Res. Rec. 2674 (2), 203–212. https://doi.org/10.1177/0361198120906423.
Wang, H., Liu, X., Zhang, H., Apostolidis, P., Erkens, S., Skarpas, A., 2020b. Micromechanical modelling of complex shear modulus of crumb rubber modified bitumen. Mater. Des. 188, 108467 https://doi.org/10.1016/j.matdes.2019.108467.
Wang, S., Cheng, D., Xiao, F., 2017. Recent developments in the application of chemical approaches to rubberized asphalt. Construct. Build. Mater. 131, 101–113. https://doi.org/10.1016/j.conbuildmat.2016.11.077.
Wang, S., Huang, W., Lin, P., Wu, Z., Kou, C., Wu, B., 2021. Chemical, physical, and rheological evaluation of aging behaviors of terminal blend rubberized asphalt binder. J. Mater. Civ. Eng. 33 (11), 04021302 https://doi.org/10.1061/(asce)mt.1943-5533.0003931.
Wang, S., Wang, Q., Li, S., 2016. Thermooxidative aging mechanism of crumb-rubber-modified asphalt. J. Appl. Polym. Sci. 133 (16), 43323 https://doi.org/10.1002/app.43323.
Wen, Y., Liu, Q., Chen, L., Pei, J., Zhang, J., Li, R., 2020. Review and comparison of methods to assess the storage stability of terminal blend rubberized asphalt binders. Construct. Build. Mater. 258 https://doi.org/10.1016/j.conbuildmat.2020.119586.
Wu, X., Formela, K., Rasool, R.t., Wang, S., 2017. Evaluation of structural change during fast transformation process of cross-linked NR into liquid NR by light pyrolysis. Polym. Degrad. Stabil. 136, 48–57. https://doi.org/10.1016/j.polymdegradstab.2016.12.009.
Wu, X., Wang, S., Dong, R., 2016. Lightly pyrolyzed tire rubber used as potential asphalt alternative. Construct. Build. Mater. 112, 623–628. https://doi.org/10.1016/j.conbuildmat.2016.02.208.
Xu, G., Kong, P., Yu, Y., Yang, J., Zhu, M., Chen, X., 2022. Rheological properties of rubber modified asphalt as function of waste tire rubber reclaiming degree. J. Clean. Prod. 332, 130113 https://doi.org/10.1016/j.jclepro.2021.130113.
Yang, X., You, Z., Perram, D., Hand, D., Ahmed, Z., Wei, W., Luo, S., 2019. Emission analysis of recycled tire rubber modified asphalt in hot and warm mix conditions. J. Hazard Mater. 365, 942–951. https://doi.org/10.1016/j.jhazmat.2018.11.080.
Yao, H., Zhou, S., Wang, S., 2015. Structural evolution of recycled tire rubber in asphalt. J. Appl. Polym. Sci. 133 (6), 42954 https://doi.org/10.1002/app.42954.
Zhao, M., Dong, R., Chi, Z., Aljarmouzi, A., Li, J., 2021. Effect of process variables on the chemical characteristics of crumb rubber desulfurized by waste cooking oil and its desulfurization mechanism. Construct. Build. Mater. 311, 125361 https://doi.org/10.1016/j.conbuildmat.2021.125361.
Zhou, T., Kabir, S.K.F., Cao, L., Fini, E.H., 2021. Effects of ultraviolet exposure on physicochemical and mechanical properties of bio-modified rubberized bitumen: sustainability promotion and resource conservation. Resour. Conserv. Recycl. 171, 105626 https://doi.org/10.1016/j.resconrec.2021.105626.